Josephson current in a normal-metal nanowire coupled to a superconductor/ferromagnet/superconductor junction

Hiromi Ebisu,[1] Bo Lu,[1] Katsuhisa Taguchi,[1,2] Alexander A. Golubov,[3,4] and Yukio Tanaka[1,4]

[1]*Department of Applied Physics, Nagoya University, Nagoya 464-8603, Japan*

[2]*Department of Physics, Hong Kong University of Science and Technology, Clear Water Bay, Hong Kong, China*

[3]*Faculty of Science and Technology and MESA+ Institute for Nanotechnology, University of Twente, 7500 AE Enschede, The Netherlands*

[4]*Moscow Institute of Physics and Technology, Dolgoprudny, Moscow 141700, Russia*

(Received 9 September 2015; revised manuscript received 18 November 2015; published 12 January 2016)

We consider a superconducting nanowire proximity coupled to a superconductor/ferromagnet/superconductor (S/F/S) junction, where the magnetization penetrates into a superconducting segment in a nanowire decaying as $\sim \exp[-\frac{|n|}{\xi}]$, where n is the site index and the ξ is the decay length. We tune chemical potential and spin-orbit coupling so that the topological superconducting regime hosting the Majorana fermion is realized for long ξ. We find that when ξ becomes shorter, zero energy state at the interface between a superconductor and a ferromagnet splits into two states at nonzero energy. Accordingly, the behavior of the Josephson current is drastically changed due to this "zero mode-nonzero mode crossover." By tuning the model parameters, we find an almost second-harmonic current-phase relation $\sin 2\varphi$, where φ is the phase difference of the junction. Based on the analysis of Andreev bound state (ABS), we clarify that the current-phase relation is determined by coupling of the states within the energy gap. We find that the emergence of crossing points of ABS is a key ingredient to generate $\sin 2\varphi$ dependence in the current-phase relation. We further study both the energy and φ dependence of pair amplitudes in the ferromagnetic region. For large ξ, an odd-frequency spin-triplet s-wave component is dominant. The magnitude of the odd-frequency pair amplitude is enhanced at the energy level of ABS.

DOI: 10.1103/PhysRevB.93.024509

I. INTRODUCTION

It is known that a number of remarkable physical phenomena occur in superconductor/ferromagnet (S/F) hybrid structures [1–3]. The first one is the generation of π state [4,5] in S/F/S junctions. Since the exchange coupling and spin-singlet Cooper pair are competing against each other, spin-singlet pairs in the ferromagnet have a spatial oscillation with changing sign in the presence of the exchange coupling [6–10]. The next one is the dominant second harmonic in the current-phase relation of the Josephson current $\sin 2\varphi$, where φ is the phase difference across the junction. It is known that $\sin 2\varphi$ dependence [11] appears near the 0-π transition point [12,13]. The third one is the generation of the odd-frequency pairing in the F region by proximity effect in S/F hybrid systems [3,14,15]. There have been many theoretical [16,17] and experimental [18–23] works about proximity effect via odd-frequency pairing in the S/F junctions. The fourth one is the so called inverse proximity effect where magnetization penetrates into a superconductor [24–27]. The electronic property and pairing symmetry near the S/F interface is drastically changed by this effect.

Independently of research directions mentioned above, study of nanowire on the surface of a superconductor in the presence of applied Zeeman magnetic field has recently become a hot topic in condensed matter physics [28,29]. Due to the strong spin-orbit coupling (SOC) in a nanowire, a topological superconducting state is generated. Then, by the bulk-edge correspondence, a superconducting nanowire hosts a Majorana fermion (MF) as the end state [28–30], which is one of the important factors to realize quantum computation [31–34]. It has also been reported that a chain of ferromagnetic atoms on a superconductor forms a topologically nontrivial state, where the ABS within the superconducting gap is localized around the edge as a MF [35–44]. The common feature in these one-dimensional topological superconducting systems is that both pair potential and magnetization coexist in all sites of the nanowire.

Up to now, although inverse proximity effect and topological superconductivity have been studied independently, they have not been studied simultaneously. It is a challenging issue to clarify an effect where both effects coexist in the same model. If we consider a proximity coupled nanowire on the S/F/S junction, we can divide the nanowire into three segments: left superconductor, middle ferromagnet, and right superconductor. Thus it is possible to design effective one-dimensional S/F/S junctions in a nanowire. We consider the situation where the ferromagnetic order of F depends on the position in the S/F/S junction. Besides, to discuss topological superconductivity, we consider Rashba-type SOC in a nanowire. If ξ which represents the penetration length of ferromagnetic order is long, the zero energy state is generated at the S/F interface. On the other hand, if ξ is short, we can expect that this zero energy state splits into two [45–47] around the magnetic impurity. Thus, a proximity coupled nanowire on the S/F/S junction is interesting since we can study both inverse proximity effect and topological superconductivity in the same model. If we tune ξ as a parameter, the present model has a unique feature to study a new type of inverse proximity effect including topological superconductivity.

In this paper we study electronic spectra and the resulting Josephson current in this nanowire S/F/S model. First, we calculate local density of states (LDOS) of an isolated left side superconducting segment where magnetization penetrates from the right edge proportional to $\exp[\frac{n}{\xi_L}]$ with site index $n < 0$ and the decay length ξ_L. We clarify that if ξ_L exceeds a certain value, LDOS has a clear zero energy peak (ZEP)

due to the zero mode at the edge. On the other hand, when ξ_L becomes shorter, LDOS has a peak splitting. We call this effect "zero mode-nonzero mode crossover." Throughout this paper we introduce zero mode and nonzero mode to distinguish zero energy state localized at the interface and splitted state. We study the Josephson current in the S/F/S nanowire junction by changing the decay length of ferromagnetic order into the left (right) side superconductor ξ_L (ξ_R), and chemical potential of the ferromagnet. It is seen that the behavior of Josephson current is quite different when the decay length becomes shorter due to the zero mode-nonzero mode crossover.

Especially when these nonzero modes [45–47] are localized at the boundary between superconductor and ferromagnet, we find an anomalous current-phase relation which can be roughly expressed as $\sin 2\varphi$. In order to understand the physical origin of the current-phase relation more clearly, we calculate the ABS and provide an argument that the emergence of crossing points of ABS is a key ingredient to produce current-phase relation $\sin 2\varphi$. This mechanism is distinct from a preexisting case in S/F/S junctions [1,11–13]. We also calculate pair amplitude decomposing into an odd-frequency part and an even-frequency one. We focus on the s-wave component of the odd-frequency spin-triplet even-parity (OTE) pairing and show their dependence on energy and phase difference φ. For a large magnitude of $\xi_{L(R)}$, an equal spin OTE pair amplitude becomes dominant and enhanced at the energy level of the ABS.

This paper is organized as follows: In Sec. II we provide the formulation to calculate LDOS and Josephson current using recursive Green's function technique. In Sec. III A we calculate LDOS on the edge of an isolated left side superconducting segment with decaying ferromagnetic order from the right edge. In Sec. III B we analyze the Josephson current in a S/F/S junction changing decay length of ferromagnetic order parameter and chemical potential of the ferromagnet. In Sec. III C we calculate ABS and discuss the relevance to the current-phase relation in Sec. III B. In Sec. III D we calculate pair amplitudes to shed light on these results from different angles. Finally, we summarize our results in Sec. IV.

II. FORMULATION

In this section we provide a formulation to calculate LDOS and Josephson current using recursive Green's function. The method of calculating ABS is also included in this section.

First, we review some general aspects of the recursive Green's function technique. Its spirit is as follows: to build the full Green's function, we start from isolated blocks and connect them to other parts of the system by stacking sites one by one along a certain direction. For example, we consider a one-dimensional atomic chain along the x direction as shown in Fig. 1(a) and suppose that the Green's function of the detached N sites on the left side has been known. We denote $G^{\mathrm{L}}_{N,N}$ as the Green's function at the N site. Consider adding one more site from the right to this system. Based on the Dyson equation, we have

$$G^{\mathrm{L}}_{N+1,N+1} = g_{\mathrm{iso}} + g_{\mathrm{iso}} V_{N+1,N} G^{\mathrm{L}}_{N,N+1}, \quad (1)$$

$$G^{\mathrm{L}}_{N,N+1} = G^{\mathrm{L}}_{N,N} V_{N,N+1} G^{\mathrm{L}}_{N+1,N+1}, \quad (2)$$

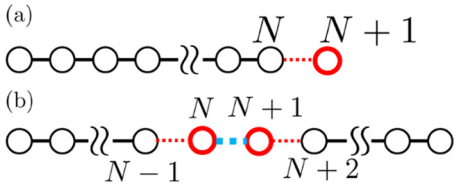

FIG. 1. (a) A schematic picture of a one-dimensional chain which is created by adding sites from left to right. (b) A schematic picture of a one-dimensional chain which is created by stacking sites both from left to right and right to left and finally connect the two chains.

where g_{iso} is the Green's function of the isolated $N+1$ site. Substituting Eq. (1) into Eq. (2) we get

$$G^{\mathrm{L}}_{N+1,N+1} = \left[g^{-1}_{\mathrm{iso}} - V_{N+1,N} G^{\mathrm{L}}_{N,N} V_{N,N+1}\right]^{-1}. \quad (3)$$

LDOS can be calculated as follows:

$$\rho^{L}(E) = -\frac{1}{\pi}\mathrm{Im}\mathrm{Tr}\left[G^{\mathrm{L}}_{N+1,N+1}(E + i0^{+})\right], \quad (4)$$

with infinitesimal positive number 0^+. Similarly, one can determine the Green's function by stacking from right to left (in this case the superscript of G is replaced with R, such as $G^{\mathrm{R}}_{N,N}$). Provided that we start this stacking process simultaneously from the two ends, we can obtain the Green's function $G^{\mathrm{L}}_{N-1,N-1}$ at site $N-1$ of the left chain and $G^{\mathrm{R}}_{N+2,N+2}$ at site $N+2$ of the right chain.

From Eq. (3) we know that the process of adding the site N in the left chain generates

$$G^{\mathrm{L}}_{N,N} = \left[g^{-1}_{\mathrm{iso}} - V_{N,N-1} G^{\mathrm{L}}_{N-1,N-1} V_{N-1,N}\right]^{-1}, \quad (5)$$

and similarly

$$G^{\mathrm{R}}_{N+1,N+1} = \left[g^{-1}_{\mathrm{iso}} - V_{N+1,N+2} G^{\mathrm{R}}_{N+2,N+2} V_{N+2,N+1}\right]^{-1}, \quad (6)$$

from adding the site $N+1$ in the right chain. Now we connect the two chains [light-blue dashed line in Fig. 1(b)] and denote the Green's function of this combined chain as G. Based on

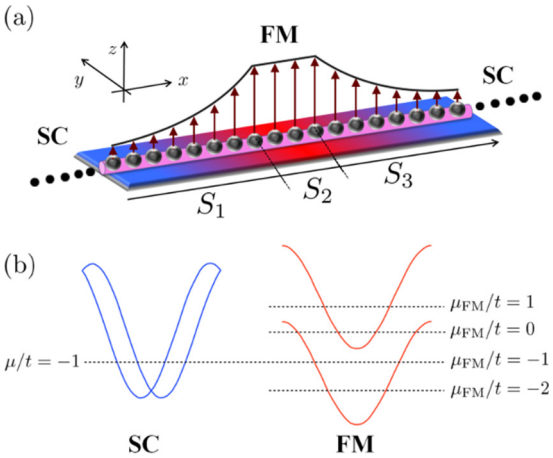

FIG. 2. (a) A schematic picture of a nanowire on top of a S/F/S junction. (b) Chemical potential of a nanowire in the superconductor segment (left) and ferromagnet segment (right).

the Dyson equation we get following equations:

$$G_{N,N} = \left[\left(G^{\mathrm{L}}_{N,N}\right)^{-1} - V_{N,N+1}G^{\mathrm{R}}_{N+1,N+1}V_{N+1,N}\right]^{-1}, \quad (7)$$

$$G_{N+1,N+1} = \left[\left(G^{\mathrm{R}}_{N+1,N+1}\right)^{-1} - V_{N+1,N}G^{\mathrm{L}}_{N,N}V_{N,N+1}\right]^{-1}, \quad (8)$$

$$G_{N,N+1} = G^{\mathrm{L}}_{N,N}V_{N,N+1}G_{N+1,N+1}, \quad (9)$$

$$G_{N+1,N} = G^{\mathrm{R}}_{N+1,N+1}V_{N+1,N}G_{N,N}. \quad (10)$$

Suppose the hopping amplitude of adjacent sites is given by t, we can calculate the current

$$J = -ietk_BT\sum_{\omega_n}\mathrm{Tr}[G_{N+1,N}(\omega_n) - G_{N,N+1}(\omega_n)], \quad (11)$$

with Boltzmann constant k_B, temperature T, and Matsubara frequency ω_n.

Next, we construct the model Hamiltonian of the semiconducting nanowire on top of the S/F/S junction [Fig. 2(a)]. We separate this nanowire into three parts by introducing

$$S_1 = \{n|1 \leqslant n \leqslant L_{\mathrm{SC}}\}, \quad S_2 = \{n|L_{\mathrm{SC}}+1 \leqslant n \leqslant L_{\mathrm{SC}}+L_{\mathrm{FM}}\}, \quad S_3 = \{n|L_{\mathrm{SC}}+L_{\mathrm{FM}}+1 \leqslant n \leqslant 2L_{\mathrm{SC}}+L_{\mathrm{FM}}\}, \quad (12)$$

with site index n. We denote the equal site length of each side of superconductors as L_{SC} and that of ferromagnet as L_{FM} . We define the Hamiltonian as follows:

$$\begin{aligned}\mathcal{H} = &-t\sum_{\substack{\langle m,n\rangle\\ \sigma}} c^\dagger_{m\sigma}c_{n\sigma} + \sum_{\substack{n\in S_1\\ n\in S_3}}\left(\frac{A}{2}c^\dagger_{n\uparrow}c_{n+1\downarrow} - \frac{A}{2}c^\dagger_{n\downarrow}c_{n+1\uparrow} + \mathrm{H.c.}\right) - \sum_{\substack{n\in S_1\\ \sigma}}\mu c^\dagger_{n\sigma}c_{n\sigma} + \sum_{n\in S_1}(\Delta c^\dagger_{n\uparrow}c^\dagger_{n\downarrow} + \mathrm{H.c.})\\ &- \sum_{\substack{n\in S_3\\ \sigma}}\mu c^\dagger_{n\sigma}c_{n\sigma} + \sum_{n\in S_3}(\Delta e^{i\varphi}c^\dagger_{n\uparrow}c^\dagger_{n\downarrow} + \mathrm{H.c.}) - \sum_{\substack{n\in S_2\\ \sigma}}\mu_{\mathrm{FM}}c^\dagger_{n\sigma}c_{n\sigma} + \sum_{n\in S_2}V_z(c^\dagger_{n\uparrow}c_{n\uparrow} - c^\dagger_{n\downarrow}c_{n\downarrow})\\ &+ \sum_{n\in S_1}V_z\exp\left[\frac{n-L_{\mathrm{SC}}}{\xi_L}\right](c^\dagger_{n\uparrow}c_{n\uparrow} - c^\dagger_{n\downarrow}c_{n\downarrow}) + \sum_{n\in S_3}V_z\exp\left[\frac{L_{\mathrm{SC}}+L_{\mathrm{FM}}+1-n}{\xi_R}\right](c^\dagger_{n\uparrow}c_{n\uparrow} - c^\dagger_{n\downarrow}c_{n\downarrow}), \end{aligned} \quad (13)$$

where $c^\dagger_{n\sigma}(c_{n\sigma})$ is the electron creation (annihilation) operator with site n and spin σ, t is the hopping matrix between the nearest neighbor $\langle i,j\rangle$, A is the strength of the Rashba SOC, $\mu(\mu_{\mathrm{FM}})$ is the chemical potential in the superconductor (ferromagnet) segment, Δ is the pair potential, φ is the phase difference of superconductors, V_z is the ferromagnetic order, and $\xi_{R(L)}$ is the decay length of ferromagnetic order in the right (left) superconductor. Unlike the model Hamiltonian on top of the superconductor with uniform ferromagnetic order, in this model construction we assume that ferromagnetic order penetrates into the right (left) superconductor segment decaying as $\sim \exp[\frac{-n}{\xi_R}]$ ($\exp[\frac{n}{\xi_L}]$) as described in Eq. (13). As for Rashba SOC, we do not include the second term in Eq. (13) at the interface between the superconductor and ferromagnet since it does not affect our results.

Now we apply the recursive Green's function technique to calculate LDOS, Josephson current, and ABS. The retarded and Matsubara Green's function of the isolated site can be described as

$$g_{\mathrm{iso}}(E) = \frac{1}{(E+i0^+) - \mathcal{H}_{\mathrm{iso}}}, \quad (14)$$

$$g_{\mathrm{iso}}(\omega_n) = \frac{1}{i\omega_n - \mathcal{H}_{\mathrm{iso}}}, \quad (15)$$

where $\mathcal{H}_{\mathrm{iso}}$ is

$$\mathcal{H}_{\mathrm{iso}} = c^\dagger_n\hat{\mathcal{H}}_{\mathrm{iso}}c_n,$$

$$\hat{\mathcal{H}}_{\mathrm{iso}} = \begin{cases} -\mu\sigma_0\tau_z - \sigma_y\tau_y\Delta, & n\in S_1,\\ -\mu_{\mathrm{FM}}\sigma_0\tau_z, & n\in S_2,\\ -\mu\sigma_0\tau_z - \sigma_y\tau_\downarrow\Delta e^{i\varphi} - \sigma_y\tau_\uparrow\Delta e^{-i\varphi}, & n\in S_3, \end{cases} \quad (16)$$

with the basis $c_n = (c_{n\uparrow}, c_{n\downarrow}, c^\dagger_{n\uparrow}, c^\dagger_{n\downarrow})$. $\sigma_{0,x,y,z}(\tau_{0,x,y,z})$ is the Pauli matrix in spin (particle-hole) space and $\tau_\uparrow = (\tau_x + i\tau_y)/2$, $\tau_\downarrow = (\tau_x - i\tau_y)/2$. The hopping matrix can be written as follows:

$$V_{n,n+1} = c^\dagger_n\hat{V}_{n,n+1}c_{n+1},$$

$$V_{n+1,n} = c^\dagger_{n+1}\hat{V}_{n+1,n}c_n,$$

$$\hat{V}_{n,n+1} = \begin{cases} -t\sigma_0\tau_z - i\frac{A}{2}\tau_z\sigma_y, & n\in S_1, n\in S_3,\\ -t\sigma_0\tau_z, & n\in S_2, \end{cases} \quad (17)$$

$$\hat{V}_{n+1,n} = \begin{cases} -t\sigma_0\tau_z + i\frac{A}{2}\tau_z\sigma_y, & n\in S_1, n\in S_3,\\ -t\sigma_0\tau_z, & n\in S_2. \end{cases} \quad (18)$$

In the next section we will calculate the LDOS on the edge of the nanowire with a proximity coupled pair potential and decaying ferromagnetic order, Josephson current, and ABS of the nanowire on a S/F/S junction. LDOS is given by

$$\rho^L(E) = -\frac{1}{\pi}\mathrm{Im}\mathrm{Tr}\left[G^L_{L_{\mathrm{SC}},L_{\mathrm{SC}}}(E+i0^+)\right]. \quad (19)$$

From Eq. (24) the Josephson current and LDOSs are described as follows:

$$J(\varphi) = -ietk_BT\sum_{\omega_n}\mathrm{Tr}[G_{n+1,n}(\omega_n) - G_{n,n+1}(\omega_n)], \quad n\in S_2, \quad (20)$$

$$\rho(E,\varphi) = -\frac{1}{\pi}\mathrm{Im}\mathrm{Tr}[G_{n,n}(E+i0^+)], \quad n\in S_2, \quad (21)$$

where φ is the macroscopic phase difference of the pair potential between two superconductors. We can calculate φ dependence explicitly.

III. RESULTS

This section consists of four parts: In Sec. III A we study the LDOS on the edge of the nanowire with both pair potential and decaying ferromagnetic order and exhibit the evolution of the surface resonance modes. In Sec. III B we then calculate Josephson current in S/F/S junctions of the nanowire with several different decay lengths. It shows that at specific parameter tuning, an anomalous current-phase relation, which can be roughly regarded as $\sin 2\varphi$, appears. In Sec. III C we calculate ABS. From the spectrum of ABS we will provide a simple argument of explanation that the emergence of crossing points of ABS is the important factor to realize the current-phase relation $\sin 2\varphi$. In Sec. III D we finally analyze the symmetry of pair amplitudes in this junction, especially focusing on odd-frequency pairing. Odd-frequency spin-triplet pairing is enhanced when the Majorana-like zero energy state is generated at the S/F (F/S) interface [48]. Throughout this section we fix the parameters as follows: $\Delta/t = 0.1, \mu/t = -1, A/t = 1, V_z/t = 1.5$. With this choice of parameters, the condition of the topological nontrivial state [29] is satisfied when ferromagnetic order is *uniform*. We set the number of sites of the superconductor segment long enough so that the effect of overlapping between two zero energy modes on the edges of the segment is negligible. In actual numerical calculation, we fix the number of sites of the superconductor segment as $L_{\rm SC} = 4000$ and the ferromagnet one as $L_{\rm FM} = 4$. To calculate the retarded Green's function, we set the infinitesimal positive number 0^+ as $0^+/t = 0.001$.

A. LDOS

In this subsection we examine the LDOS on the edge of nanowire which is calculated from Eq. (19). The situation is illustrated in Fig. 3(a), where the pair potential and decaying ferromagnetic order coexist. The intensity of LDOS is plotted in Fig. 3(b). It is shown that for the long decaying of V_z ($\xi_L > 10$) there is a single resonance peak at zero energy. This is in agreement with the finding that in the asymptotic scenario when V_z is spatially *uniform* at infinite ξ_L, such nanowire is topologically nontrivial, which can be confirmed by the sign of Pfaffian with our choice of parameters [31]. However, in the presence of a spatially *nonuniform* ferromagnetic order, the preexisting topological argument is no longer valid. Thus, it is remarkable to see here that even if the ferromagnetic order is nonuniform, LDOS with zero energy peak can still appear on the edge of the nanowire within the numerical accuracy. On the opposite, with the decay length less than around $\xi_L \sim 10$, this zero mode splits into two resonance peaks symmetric to zero energy. Owing to the localized ferromagnet at the end of the nanowire, this finding associates with another important physical results known as Shiba states [45–47]. It is well known that when a magnetic impurity is put on the superconductor, there is a bound state around the impurity inside the superconducting energy gap. In the present model we can control the zero mode-nonzero mode crossover with decreasing the decay

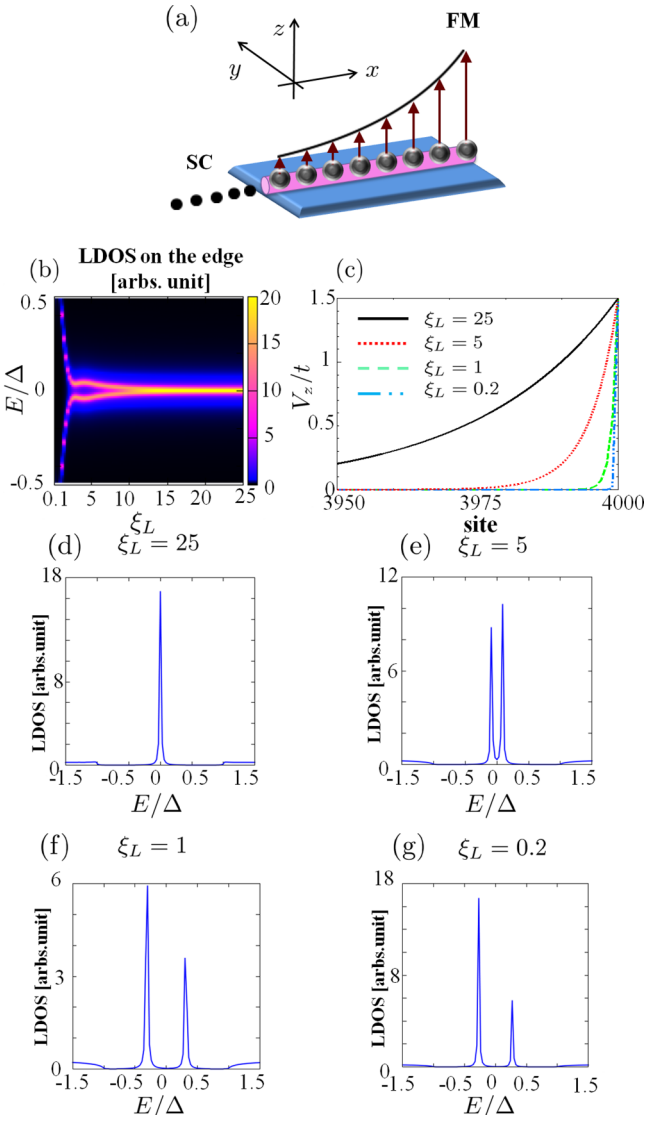

FIG. 3. (a) A schematic picture of a nanowire on top of a superconductor with decaying ferromagnetic order. (b) The intensity plot of LDOS on the edge (i.e., $n = L_{\rm SC}$) of the nanowire shown in (a). (c) The spatial profiles of ferromagnetic order with different decay lengths, $\xi_L = 25$ (black solid line), $\xi_L = 5$ (red dotted line), $\xi_L = 1$ (green dashed line), and $\xi_L = 0.2$ (blue two-dotted line). (d)–(g) LDOS on the edge of the nanowire with different decay lengths.

length of ferromagnetic order. In Figs. 3(d)–3(g) we plot the LDOS for a selected decay length $\xi_L = 25$, 5, 1, and 0.2, respectively [see also Fig. 3(c) where the spatial profiles of ferromagnetic order are shown for four different decay lengths]. When $\xi_L = 25$, we see the zero energy mode, on the other hand, in the rest of the cases [Figs. 3(e)–3(g)], we find nonzero modes in the energy gap of the superconducting region.

In the Appendix we consider the overlapping of two zero energy modes in the shorter length system and also compare the nonuniform ferromagnetic case and uniform case, which leads that two zero energy modes appearing in a nonuniform situation can be regarded as two MFs.

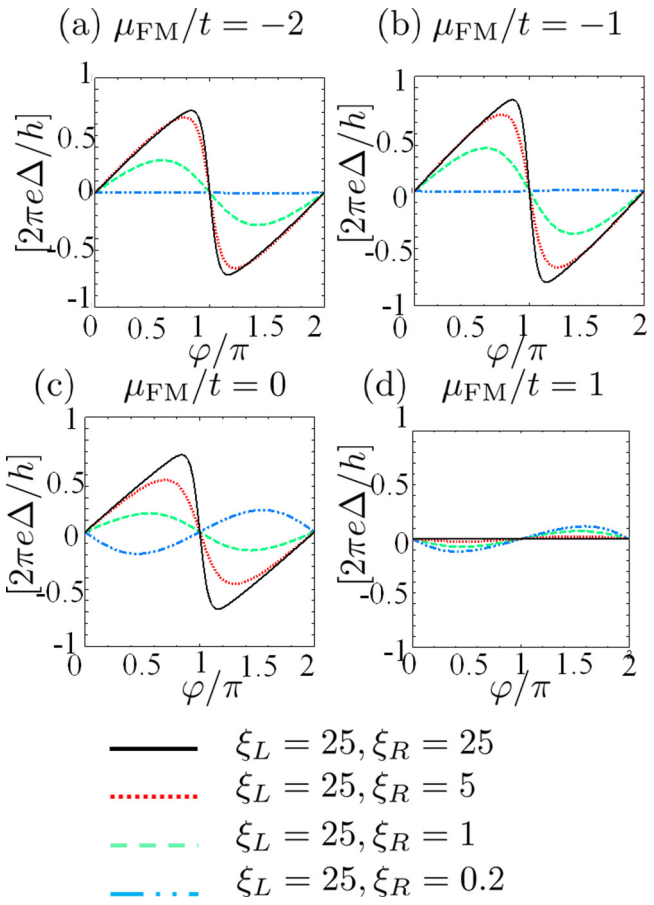

FIG. 4. (a)–(d) Josephson current of the nanowire on top of a S/F/S junction in the case of $\xi_L = 25$ with four different chemical potentials of ferromagnetic layer listed above each figure. There are four lines in each figure: $\xi_L = 25, \xi_R = 25$ (black solid line), $\xi_L = 25, \xi_R = 5$ (red dashed line), $\xi_L = 25, \xi_R = 1$ (green dashed line), and $\xi_L = 25, \xi_R = 25$ (blue two-dotted line).

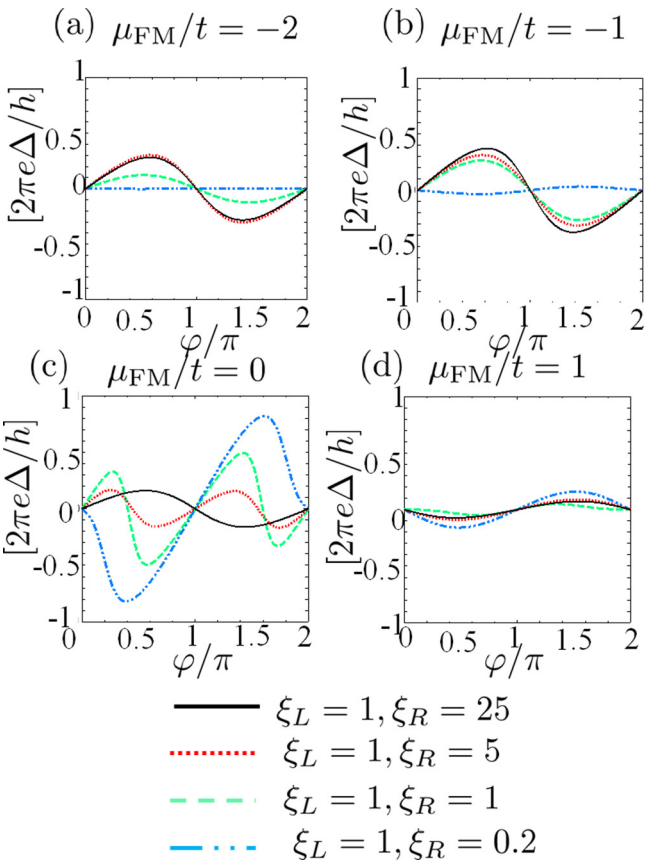

FIG. 5. (a)–(d) Josephson current of the nanowire on top of a S/F/S junction in the case of $\xi_L = 1$ with four different chemical potentials of ferromagnetic layer listed above each figure. There are four lines in each figure: $\xi_L = 1, \xi_R = 25$ (black solid line), $\xi_L = 1, \xi_R = 5$ (red dashed line), $\xi_L = 1, \xi_R = 1$ (green dashed line), and $\xi_L = 1, \xi_R = 0.2$ (blue two-dotted line).

B. Josephson current

In this subsection we study Josephson currents for various decay lengths of ferromagnetic order on both sides of the superconductor. On the left side we are interested in three typical decay lengths $\xi_L = 25$, 1, and 0 (i.e., ferromagnetic order does not penetrate into the left superconductor). In each case we will tune the decay length ξ_R as well as the chemical potential of the ferromagnet segment [$\mu_{\rm FM}/t = -2,\ -1,\ 0,$ and 1, see also Fig. 2(b)].

First, we look at the case $\xi_L = 25$. As the previous discussion shows, there is a zero energy mode on the edge of the left nanowire. In Figs. 4(a)–4(d) we plot Josephson currents for $\mu_{\rm FM}/t = -2,\ -1,\ 0,$ and 1, respectively. In each figure we take four values of $\xi_R = 25,\ 5,\ 1,$ and 0.2. The phase dependence of the current in all cases has the dominant coupling proportional to $\sin\varphi$. Interestingly, for $\mu_{\rm FM}/t = -2,\ -1,$ and 0, the Josephson current in symmetric junctions abruptly changes its sign at $\varphi = \pi$, as shown in Figs. 4(a), 4(b), and 4(c), respectively. In asymmetric junctions, such a jump is absent. Notice that our system considered here has no perfect transmissivity and is closely similar to that of two d-wave superconductors with zero energy ABSs [49–51], p-wave superconductors [52,53], or a Kitaev chains junction system where MFs are coupled with each other [31,54]. Therefore, the abrupt jump can only be explained by the existence of robust zero energy ABSs [55–59], i.e., MFs [31]. However, in the nonuniform ferromagnetic order, the formation of zero modes are distinct from the p-wave superconductor or Kitaev model. It is interesting that the similar behavior of Josephson current is found even in the present model. For $\mu_{\rm FM}/t = 1$ we obtain a π state and the current are quite small compared to the other cases of chemical potentials. In this case there is one band at the chemical potential in the ferromagnetic region which has opposite spin compared to the ferromagnetic order in SCs. Thus, the transparency of the junction is greatly reduced and the π state can appear as a result of misaligned magnetizations.

Second, we focus on the case $\xi_L = 1$ where nonzero modes are localized on the left segment. As for $\mu_{\rm FM}/t = -2$ and -1 [Figs. 5(a) and 5(b)], we find the current-phase relation $\sin\varphi$ in three cases: $\xi_R = 25$ (black solid line), $\xi_R = 5$ (red dotted line), and $\xi_R = 1$ (green dashed line). On the other hand, Josephson current is almost zero when $\xi_R = 0.2$ (blue two-dashed line). Surprisingly, when $\mu_{\rm FM}/t = -2$, $\xi_R = 5$ and $\xi_R = 1$ [Fig. 5(c) red dotted and green dashed lines], we find the anomalous current-phase relation which can be roughly

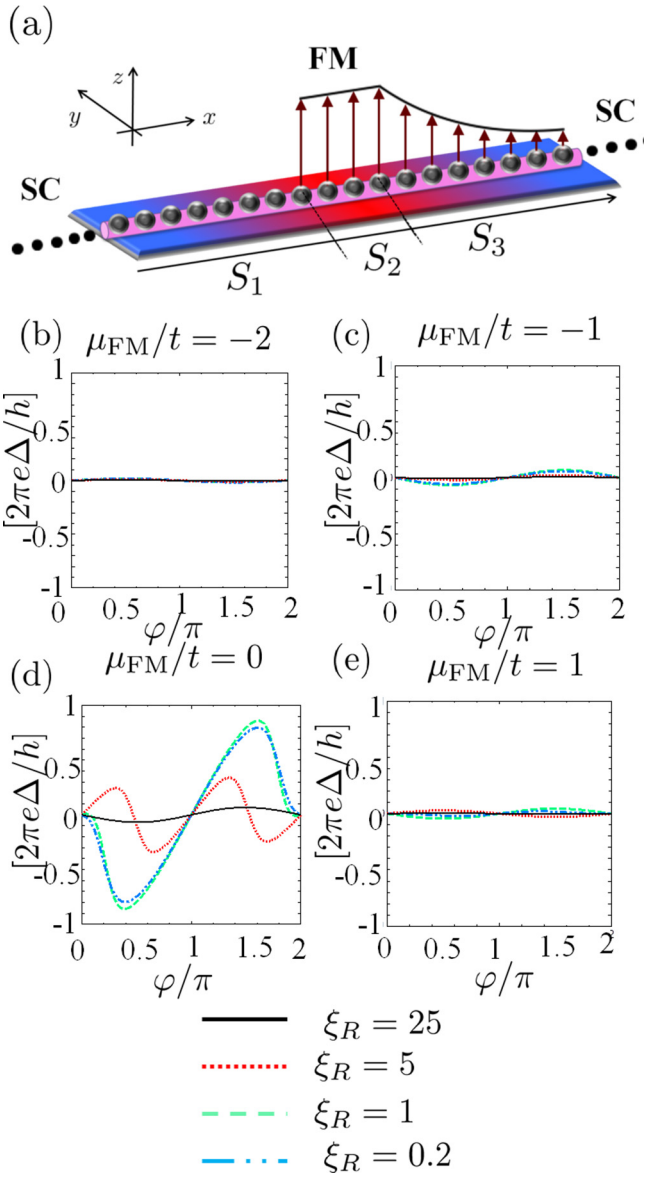

FIG. 6. (a) A schematic picture of a nanowire on top of a S/F/S junction. (a)–(d) Josephson current of the nanowire on top of a S/F/S junction in the case of $\xi_L = 0$, that is, ferromagnetic order does not penetrate into the left superconductor segment. Results are shown with four different chemical potentials of ferromagnetic layer listed above each figure. There are four lines in each figure: $\xi_L = 0, \xi_R = 25$ (black solid line), $\xi_L = 0, \xi_R = 5$ (red dashed line), $\xi_L = 0, \xi_R = 1$ (green dashed line), and $\xi_L = 0, \xi_R = 25$ (blue two-dotted line).

regarded as $\sin 2\varphi$. As we will see in the next subsections, the coupling of nonzero modes produces this anomalous current-phase relation especially when the emergence of crossing points of ABS becomes the important factor. For $\mu_{\rm FM}/t = 1$, all of the Josephson currents are suppressed compared to the other cases of chemical potential.

Finally, we study the case $\xi_L = 0$, i.e., the ferromagnetic order does not penetrate into the left superconductor segment. When $\mu_{\rm FM}/t = -2, -1$, and 1 [Figs. 6(b), 6(c), and 6(d), respectively), the Josephson current is almost zero, on the other hand, when $\mu_{\rm FM}/t = 0$, we see the current-phase relation $\sin 2\varphi$ with decay length on the right $\xi_R = 5$ (dotted red line) and $-\sin\varphi$ with other decay length.

Before we proceed, it is instructive to summarize the interesting phenomena we have found in this subsection. In the case of $\xi_L = 25$ and $\mu_{\rm FM}/t = -2, -1$, and 0 we see the abrupt sign reversal of current at $\varphi = \pi$. In the case of $\xi_L = 25$ and $\mu_{\rm FM}/t = 1$, the amplitude of Josephson current is suppressed. When $\xi_L = 1$, $\mu_{\rm FM}/t = 0$, and $\xi_R = 5$ or 1, we obtain the current-phase relation approximated as $\sin 2\varphi$. We also find this current-phase relation $\sin 2\varphi$ in the case of $\xi_L = 0$, $\mu_{\rm FM}/t = 0$, and $\xi_R = 5$.

C. ABS

In this subsection we study the ABS of nanowire on a S/F/S junction with different decay lengths and relate it to the behavior of the Josephson current obtained in the previous subsection. We mainly focus on the case of $\mu_{\rm FM}/t = 0$. It is well known that when the magnitudes of the pair potential are the same on the left and right side of the superconductor, the Josephson current can be calculated by

$$J(\varphi) = \frac{2e}{h}\frac{\partial F(\varphi)}{\partial\varphi}, \tag{22}$$

where F is free energy. In one dimension, F can be written as

$$F = -k_B T \sum_n \log\left[2\cosh\left(\frac{\varepsilon_n}{2k_B T}\right)\right], \tag{23}$$

where ε_n is the energy of ABS [60]. Therefore, the Josephson current is

$$J(\varphi) = -\sum_n \frac{e}{h}\tanh\left(\frac{\varepsilon_n}{2k_B T}\right)\frac{\partial\varepsilon_n}{\partial\varphi}. \tag{24}$$

At low temperature, $J(\varphi)$ can be approximated as

$$J(\varphi) \sim -\frac{e}{h}\sum_n \mathrm{sgn}(\varepsilon_n)\frac{\partial\varepsilon_n}{\partial\varphi}. \tag{25}$$

$\mathrm{sgn}(\varepsilon_n)$ gives $+1$ (-1) when ε_n is positive (negative). In the above, n denotes the band index of ABS. Due to the particle-hole symmetry, we can only take the ABSs below the zero energy into account. Thus, the Josephson current can be approximated as the derivative of ABSs below the zero energy.

First, we look at the case $\xi_L = \xi_R = 25$ where the zero energy modes are located on both sides. These two zero modes hybridize as indicated in Fig. 7(a). The crossing point at $\varphi = \pi$ explains the sudden drop of Josephson current which can lead to the unusual 4π periodicity of the current-phase relation if we consider ac Josephson current. As the decay length on the right decreases, the zero energy mode on the left does not hybridize with the states on the right, which can be seen from the flat ABS as a function of φ in Figs. 7(b)–7(d). The contribution of Josephson current is mainly carried by the ABSs away from zero energy. With this estimation we can relate ABS to the behavior of the Josephson current in the previous subsection. If we look at Figs. 7(b) and 7(c) [Fig. 7(d)], ABSs below the zero energy change as $\sim -\cos\varphi$ ($\sim \cos\varphi$), which leads to current-phase relation $\sin\varphi$ ($-\sin\varphi$). This consideration corresponds

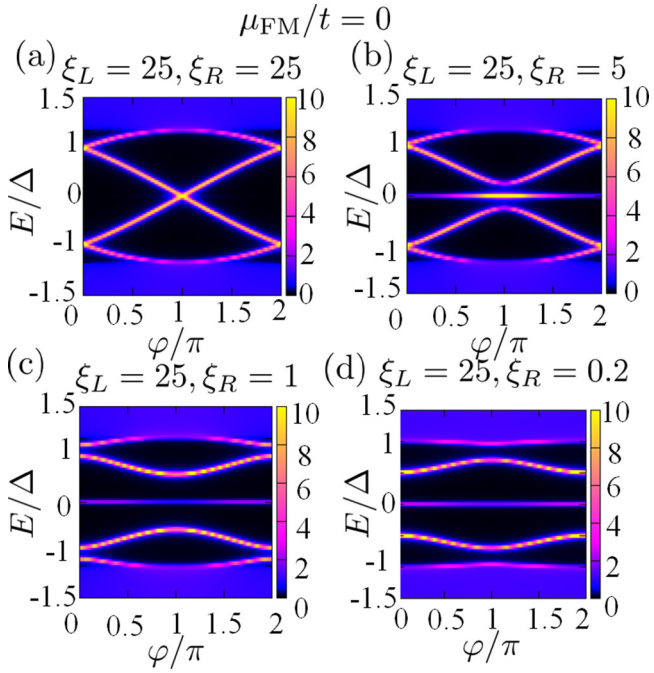

FIG. 7. (a)–(d) ABS (the intensity plot of LDOS at the ferromagnet segment within the superconducting energy gap) in the case of $\mu_{\rm FM}/t = 0$ and $\xi_L = 25$ with different decay length ξ_R.

well to the black solid line and red dotted line (green dashed line) in Fig. 4(c). If we tune the chemical potential of the ferromagnetic layer as $\mu_{\rm FM}/t = 1$, the ABSs are almost flat, which do not make a contribution to the Josephson current (Fig. 8). Indeed, the amplitude of Josephson currents are almost zero as shown in Fig. 4(d).

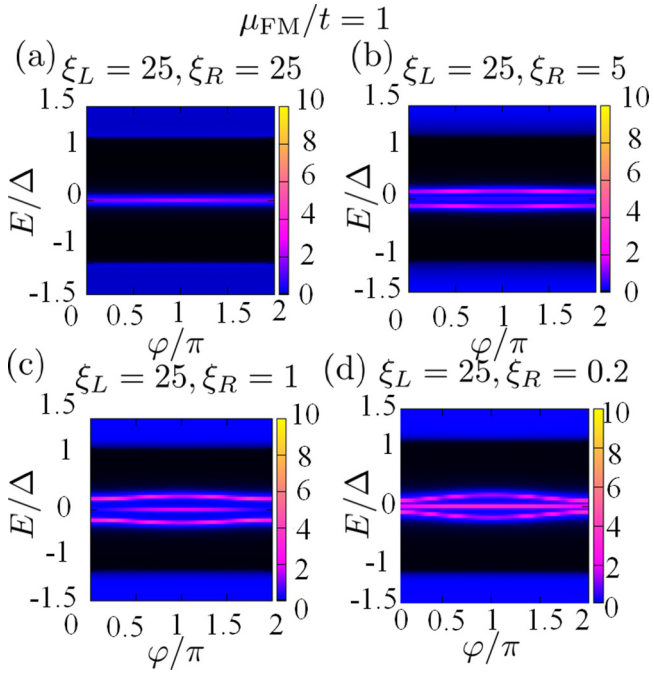

FIG. 8. (a)–(d) ABS (the intensity plot of LDOS at the ferromagnet segment within the superconducting energy gap) in the case of $\mu_{\rm FM}/t = 1$ and $\xi_L = 25$ with different decay length ξ_R.

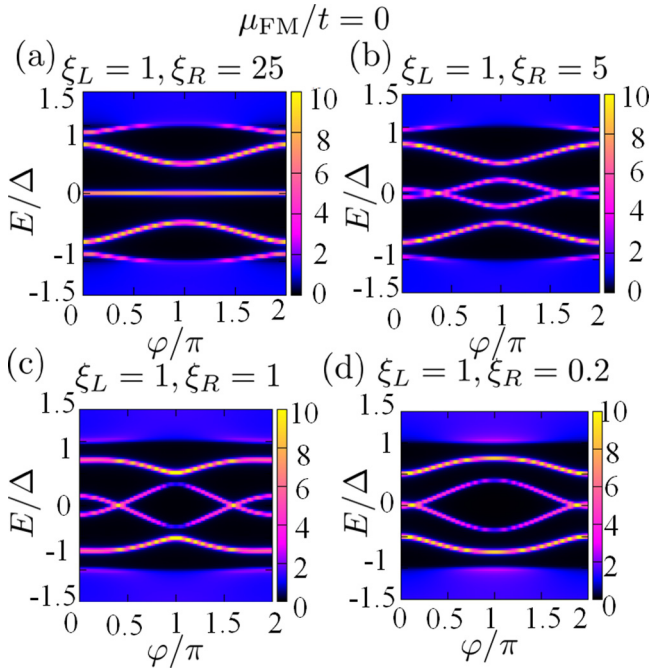

FIG. 9. (a)–(d) ABS (the intensity plot of LDOS at the ferromagnet segment within the superconducting energy gap) in the case of $\mu_{\rm FM}/t = 0$ and $\xi_L = 1$ with different decay length ξ_R.

Next, we focus on the case $\xi_L = 1$, when nonzero modes are localized at the interface between the left superconductor and ferromagnet segment. When decay length $\xi_R = 25$ [Fig. 9(a)], the zero energy mode is located on the right segment. This mode is not coupled with the left nonzero modes. The major change of ABSs below the zero energy can be regarded as $\sim -\cos\varphi$ [Fig. 9(a)] which contributes $\sin\varphi$ to the Josephson current [Fig. 5(c) black solid line].

In the case of $\xi_R = 5$ and $\xi_R = 1$, when the anomalous current-phase relation $\sin 2\varphi$ can be seen, we find that nonzero modes on both sides hybridize and these states are crossed at two values of φ: one is located between $\varphi = 0$ and π, and another is between $\varphi = \pi$ and $\varphi = 2\pi$ [Figs. 9(b) and 9(c)]. As we discuss later, this crossing point of ABS is important to realize the current-phase relation $\sin 2\varphi$. For $\xi_R = 0.2$, all of the ABSs change as $\cos\varphi$ [Fig. 9(d)], which gives current-phase relation $\sin\varphi$ [Fig. 5(c) blue two-dotted line].

Finally, we focus on the case $\xi_L = 0$, i.e., ferromagnetic order is absent in the left superconductor side (Fig. 10). If we set $\xi_R = 25$, all of the ABSs becomes flat as a function of φ, which leads to almost zero Josephson current [Fig. 6(c) black solid line]. For $\xi_R = 1$ and 0.2 the change of ABS below the zero energy obeys $\sim \cos\varphi$ [Figs. 10(c) and 10(d)], thus the current-phase relation is $-\sin\varphi$ [Fig. 6(c) green dashed line and blue two-dotted line]. On the other hand, in the case of $\xi_R = 5$, when we see the current-phase relation $\sin 2\varphi$, we again find two crossing points of ABS [Fig. 10(b)].

From these analyses explained above, we find that the behavior of the Josephson current can be determined by the hybridization of ABSs and when this hybridization produces the two crossing points at the zero energy, the current-phase relation $\sin 2\varphi$ can be seen. Now we consider the simplified situation where there are two crossing points of ABSs: we

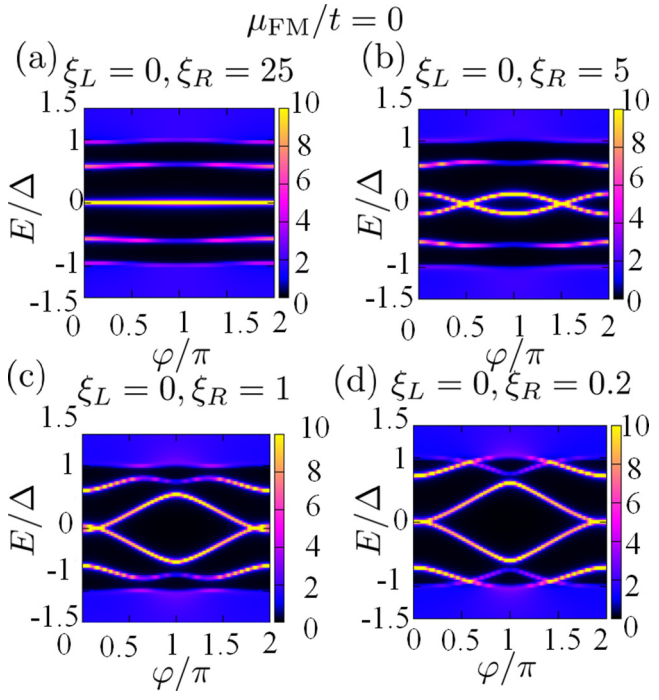

FIG. 10. (a)–(d) ABS (the intensity plot of LDOS at the ferromagnet segment within the superconducting energy gap) in the case of $\mu_{\rm FM}/t = 0$ and $\xi_L = 0$ (i.e., there is no ferromagnetic order in the left superconductor segment) with different decay length ξ_R.

have only two states within the energy gap (blue area in Fig. 11 top) which are labeled by ε_A and ε_B (Fig. 11 top). We assume ε_A (ε_B) is written as $\sim -\cos\varphi$ ($\cos\varphi$) and crossing points are located at $\varphi = \frac{\pi}{2}$ and $\frac{3\pi}{2}$. According to Eq. (25) and

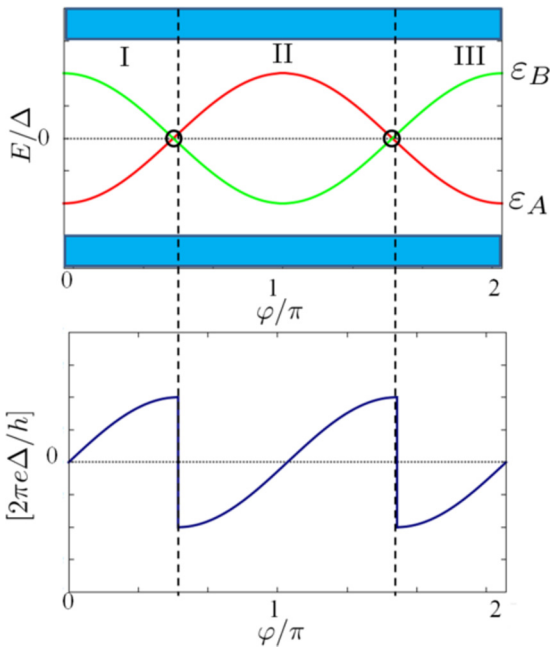

FIG. 11. Top: A schematic picture of two ABSs denoted by ε_A (red) and ε_B (green). These two states have two crossing points (solid circle) at $E = 0$. Bottom: A Josephson current which is given by $J(\varphi) \sim -\frac{\partial\varepsilon_A}{\partial\varphi}\mathrm{sgn}(\varepsilon_A)$.

particle-hole symmetry, we can focus on the states below the zero energy to estimate the Josephson current. We separate the region of φ into three: I $\{\varphi|0 \leqslant \varphi < \frac{\pi}{2}\}$, II $\{\varphi|\frac{\pi}{2} \leqslant \varphi < \frac{3\pi}{2}\}$, and III $\{\varphi|\frac{3\pi}{2} \leqslant \varphi < 2\pi\}$ (Fig. 11 top). In I and III, ABS below the zero energy obeys $-\cos\varphi$, thus Josephson current reads $\sim \sin\varphi$, while in II, ABS transforms into $\sin\varphi$, which gives Josephson current $-\sin\varphi$. We plot the Josephson current as a function of φ ($0 \leqslant \varphi < 2\pi$) in the bottom of Fig. 11. Due to the different curve that ABS obeys in I and II (II and III), there is a jump at the boundary between I and II (II and III) which generates the current-phase relation $\sin 2\varphi$. Up to now, $\sin 2\varphi$ dependence of the Josepshon current has been discussed in a S/ferromagnetic insulator/S junction [11], S/F/S with diffusive F near the vicinity of the 0-π transition point [1,12,13], d-wave superconductor junctions [49,50,61,62], and s-wave/spin triplet p-wave superconductor junctions [52,61]. Our setup of realizing $\sin 2\varphi$ dependence is distinct from the preexisting cases.

D. Symmetries of a Cooper pair

In this subsection we focus on the symmetry of a Cooper pair in the present one-dimensional S/F/S junctions. In an odd-frequency pairing state, the pair amplitude changes its sign with the exchange of times of two paired electrons [63]. Taking account of this symmetry class, symmetry of a Cooper pair is classified into (1) even-frequency spin-singlet even-parity (ESE), (2) even-frequency spin-triplet odd-parity (ETO), (3) odd-frequency spin-triplet even-parity (OTE) [63], and (4) odd-frequency spin-singlet odd-parity (OSO) [64]. Although an odd-frequency bulk superconductor has not been discovered up to now, an odd-frequency pair amplitude can exist ubiquitously as a subdominant state. It is known that odd-frequency pairing is induced by the breaking of the translational [65–67] or spin-rotational symmetry [3,14,15] from a bulk even-frequency pair potential. Also, it has been clarified that zero-energy local density of states is enhanced by the odd-frequency pairing [65,66,68–71]. Odd-frequency pairing influences seriously the proximity effect and various electronic properties of the junctions.

In the present nanowire S/F/S junctions, the symmetry of a pair amplitude far from the S/F (F/S) interface is an ESE s-wave one, since the induced pair potential is a conventional spin-singlet s wave. Due to the symmetry breaking, near the S/F (F/S) interface or inside the ferromagnet region, odd-frequency pairings can be induced. Here we focus on the s-wave component of ESE and OTE pair amplitudes in a ferromagnet region. First we focus on the real frequency representation of pair amplitudes. ESE and OTE amplitudes are given by

$$f_{\rm even}(E) = \tfrac{1}{2}\{F^{\uparrow,\downarrow}_{n,n}(E + i0^+) + F^{\uparrow,\downarrow}_{n,n}(-E - i0^+)\}, \quad (26)$$

$$f^{\sigma,\sigma'}_{\rm odd}(E) = \tfrac{1}{2}\left\{F^{\sigma,\sigma'}_{n,n}(E + i0^+) - F^{\sigma,\sigma'}_{n,n}(-E - i0^+)\right\}, \quad (27)$$

with $n \in S_2$. $F^{\sigma,\sigma'}_{n,n}$ comes from Eq. (7):

$$G_{n,n} = \begin{pmatrix} G & F \\ \tilde{F} & \tilde{G} \end{pmatrix}, \quad F = \begin{pmatrix} F^{\uparrow,\uparrow}_{n,n} & F^{\uparrow,\downarrow}_{n,n} \\ F^{\downarrow,\uparrow}_{n,n} & F^{\downarrow,\downarrow}_{n,n} \end{pmatrix}. \quad (28)$$

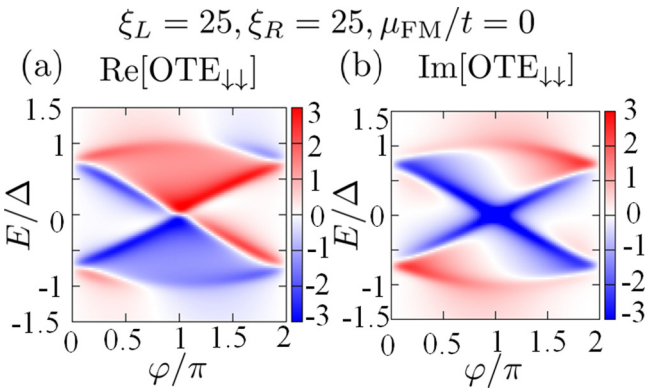

FIG. 12. (a) and (b) The intensity plot of real part (a) and imaginary part (b) of an odd-frequency spin-triplet even-parity (OTE) pair amplitude with $\downarrow\downarrow$ spin component $f_{\rm odd}^{\downarrow,\downarrow}(E)$ in the case of $\xi_L = 25$, $\xi_R = 25$, and $\mu_{\rm FM}/t = 0$.

The above representation is useful to compare with the ABS. To clarify the relation between the ABS and the pair amplitude is an interesting issue, since it has been revealed that there is a close relation between ABS and odd-frequency pairing. In the presence of zero energy ABS as a surface state of unconventional superconductors, odd-frequency pair amplitude is hugely enhanced [65,66,72,73]. Thus the presence of zero energy state (ZES) can be interpreted as an emergence of odd-frequency pairing. Also, it has been clarified that MF always accompanies odd-frequency pairing [48,74–76].

First, we calculate the pair amplitude for $\xi_L = 25$, $\xi_R = 25$, and $\mu_{\rm FM}/t = 0$. The corresponding ABS with the hybridization of Majorana-like ZESs on left and right side has been shown in Fig. 7(a). In this case, OTE pairing becomes dominant for any phase difference. As compared to other components, $f_{\rm odd}^{\uparrow,\uparrow}(E)$, $f_{\rm odd}^{\uparrow,\downarrow}(E)$, and $f_{\rm even}(E)$, the magnitude of $f_{\rm odd}^{\downarrow,\downarrow}(E)$ is dominant. This is because the direction of the majority spin in the ferromagnet is down. Therefore, we plot s-wave OTE pairing $f_{\rm odd}^{\downarrow,\downarrow}(E)$ in the middle of the ferromagnet in Fig. 12. The energy and φ dependence of $f_{\rm odd}^{\downarrow,\downarrow}(E)$ is almost similar to those of ABS in Fig. 7. For $\varphi = 0$, π, and 2π, ${\rm Re}[f_{\rm odd}^{\downarrow,\downarrow}(E)] = -{\rm Re}[f_{\rm odd}^{\downarrow,\downarrow}(-E)]$ and ${\rm Im}[f_{\rm odd}^{\downarrow,\downarrow}(E)] = {\rm Im}[f_{\rm odd}^{\downarrow,\downarrow}(-E)]$. These relations of odd-frequency pairing are known in the previous study in normal metal/superconductor junctions [77].

Next, we look at the case with $\xi_L = \xi_R = 1$ and $\mu_{\rm FM} = 0$. The corresponding ABS with double crossing points in the energy spectrum of ABS has been shown in Fig. 9(c). Such a characteristic also appears in the intensity plot of $f_{\rm odd}^{\downarrow,\downarrow}(E)$, $f_{\rm odd}^{\uparrow,\downarrow}(E)$, and $f_{\rm even}(E)$. The E and φ dependencies of $f_{\rm odd}^{\uparrow,\uparrow}(E)$ are similar to those of $f_{\rm odd}^{\downarrow,\downarrow}(E)$. The remarkable point here is that not only the odd-frequency pair amplitude but also the even-frequency pair amplitude exists with the same order in contrast to the case in Fig. 13. For $\varphi = 0$, π, and 2π, ${\rm Re}[f_{\rm odd}^{\sigma,\sigma'}(E)] = -{\rm Re}[f_{\rm odd}^{\sigma,\sigma'}(-E)]$ and ${\rm Im}[f_{\rm odd}^{\sigma,\sigma'}(E)] = {\rm Im}[f_{\rm odd}^{\sigma,\sigma'}(-E)]$, with $\sigma = \uparrow$ ($\downarrow$) and $\sigma' = \uparrow$ ($\downarrow$). On the other hand, ${\rm Re}[f_{\rm even}(E)] = {\rm Re}[f_{\rm even}(-E)]$ and ${\rm Im}[f_{\rm odd}(E)] = -{\rm Im}[f_{\rm odd}(-E)]$ are satisfied.

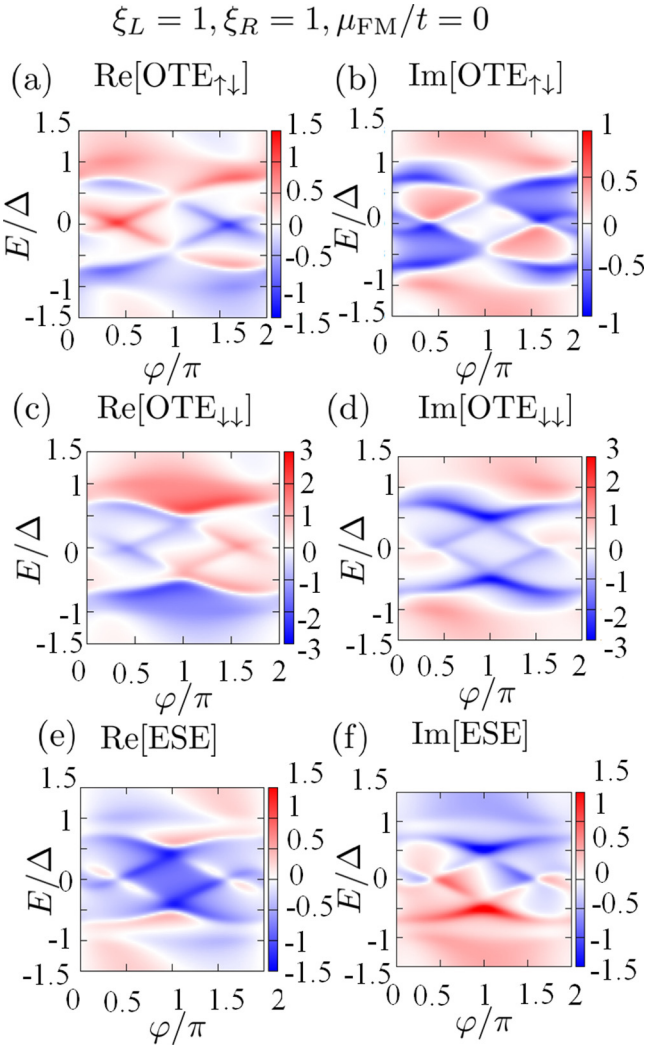

FIG. 13. (a)–(d) The intensity plot of real part (a) [(c)] and imaginary part (b) [(d)] of the odd-frequency spin-triplet even-parity (OTE) pair amplitude with $\downarrow\downarrow$ spin component $f_{\rm odd}^{\downarrow,\downarrow}(E)$ and $\downarrow\downarrow$ spin component $f_{\rm odd}^{\uparrow,\downarrow}(E)$. In (e) and (f) real part and imaginary part of the even-frequency spin-singlet pair amplitude $f_{\rm even}(E)$ is plotted.

IV. SUMMARY AND CONCLUSIONS

In this paper we have studied LDOS, a current-phase relation of Josephson current, energy levels of Andreev bound state, and induced odd-frequency pairings in a superconductor/ferromagnet/superconductor nanowire junction, where the magnetization penetrates into a superconducting segment with a decay length ξ. We have chosen the chemical potential and SOC so that the topological superconducting regime hosting MF is realized for a sufficiently large magnitude of ξ. We have found that when ξ becomes larger, LDOS has a ZEP. On the other hand, if ξ is shorter, zero energy state at the interface between a superconductor and ferromagnet splits into two states. Accordingly, the behavior of the Josephson current drastically changes. By tuning the parameters of the model, we have found an almost second-harmonic current-phase relation $\sin 2\varphi$, with phase difference φ. Based on the analysis of ABS, we clarify that the current-phase relation is determined by coupling of the states within the energy gap. We find that

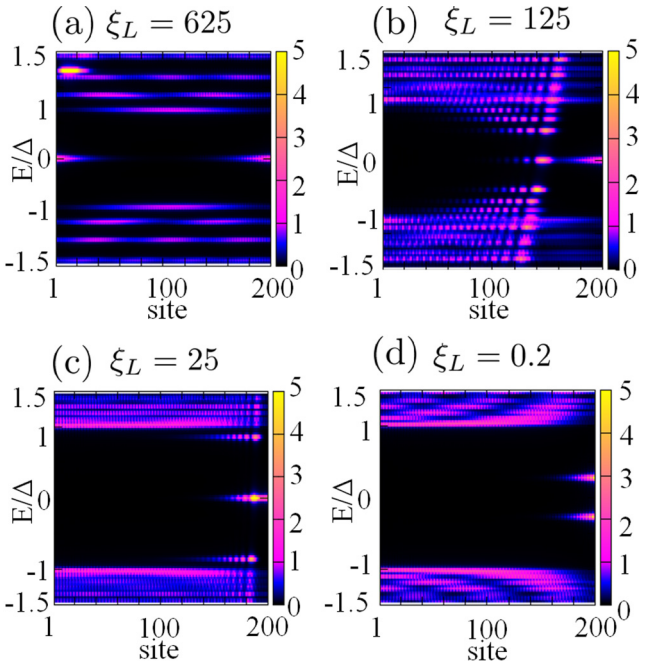

FIG. 14. (a)–(d) The intensity plot of LDOS of the nanowire with decaying ferromagnetic order on top of the superconductor. The ferromagnetic order decays from right to left similarly to Fig. 3(a). The horizontal axis represents the site index and the vertical one does energy. Decay length of the ferromagnetic order is set as (a) $\xi_L = 625$, (b) $\xi_L = 125$, (c) $\xi_L = 25$, and (d) $\xi_L = 0.2$.

the emergence of crossing points of ABS is a key ingredient to generate $\sin 2\varphi$ dependence in the current-phase relation. We further studied both the energy and φ dependence of pair amplitudes in the ferromagnet region. For long ξ, an odd-frequency s-wave triplet component is dominant. The magnitude of the odd-frequency pair amplitude is enhanced at the energy level of ABS. On the other hand, when ξ becomes shorter, not only odd-frequency pairing but also even-frequency pairing mixes.

Recently, $\sin 2\varphi$ behavior has been observed in S/F/S junctions [78], when the ferromagnet is an insulator which has a spin filter effect. Thus to clarify the relevance of our obtained $\sin 2\varphi$ dependence to this experimental report is a challenging issue. In our paper ballistic transport is assumed. If the ferromagnet becomes diffusive, we can expect anomalous proximity effect [53,79–83] by odd-frequency spin-triplet s-wave pairing. Extension to this direction is also an interesting future study.

ACKNOWLEDGMENTS

We thank J. Klinovaja, K. T. Law, K. Kawai, and S. Kawabata for fruitful discussion. This work was supported by a Grant-in-Aid for Scientific Research on Innovative Areas Topological Material Science (Grant No. 15H05853), a Grant-in-Aid for Scientific Research B (Grant No. 15H03686), a Grant-in-Aid for Challenging Exploratory Research (Grant No. 15K13498) from the Ministry of Education, Culture, Sports, Science, and Technology, Japan (MEXT); the Core Research for Evolutional Science and Technology (CREST) of the Japan Science and Technology Corporation (JST); Japan-RFBR JSPS Bilateral Joint Research Projects/Seminars (Grants No. 15-52-50054 and No. 15668956); and Dutch FOM and the Ministry of Education and Science of the Russian Federation, Grant No. 14.Y26.31.0007. K.T. and H.E. are supported by a Grant-in-Aid for JSPS Fellows (Grants No. 13J03141 and No. 15J00565).

APPENDIX: SPATIAL PROFILE OF LDOS

In this Appendix we show a spatial profile of LDOS of a superconductor with decaying ferromagnetic order to understand "zero mode-nonzero mode crossover" more clearly. The ferromagnetic order decays from right to left similarly to Fig. 3(a). Since we will consider hybridization of two ZESs on both edges of a superconductor, we set the number of sites rather short, 200.

These profiles are shown in Fig. 14. For a long enough decay length [Fig. 14(a)], ZEPs are localized on both sides of the nanowire, which is analogous to the situation where MFs are localized on both edges of the topological superconductor [44]. If the decay length is decreased, however, the zero energy mode on the left comes close to the that on the right edge [Fig. 14(b)],

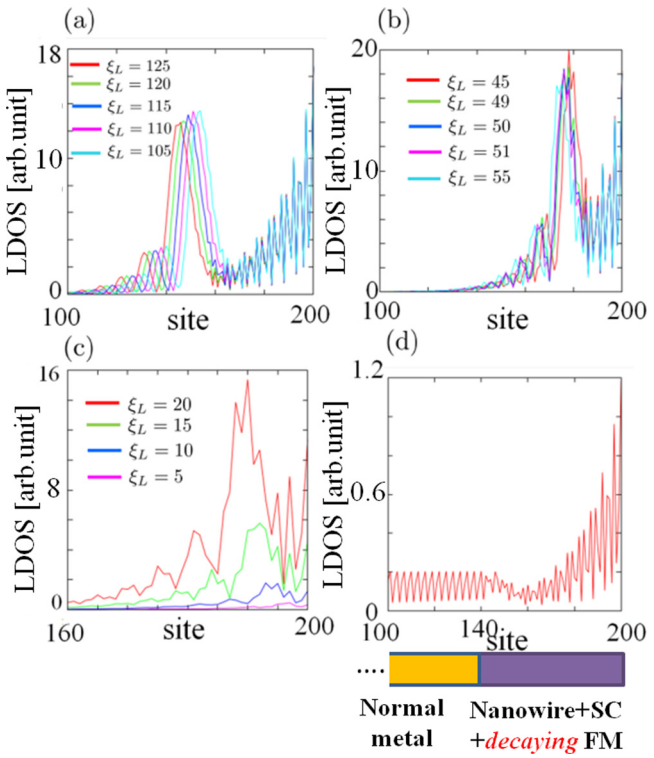

FIG. 15. (a)–(c) The spatial dependence of LDOS at zero energy of the semiconducting nanowire with pair potential and decaying ferromagnetic order whose length is 200 sites. The several cases of LDOS are plotted for different decay lengths which is indicated by different colors as shown in each figure. (d) The spatial dependence of LDOS of the normal metal/nanowire junction system. The total length of this junction is set as 200 sites and the interface between normal metal and nanowire is located at site 140. In the nanowire segment, the pair potential and decaying ferromagnetic order with $\xi_L = 125$ are also included similarly to (a)–(c). A schematic picture of this junction is shown below the plot.

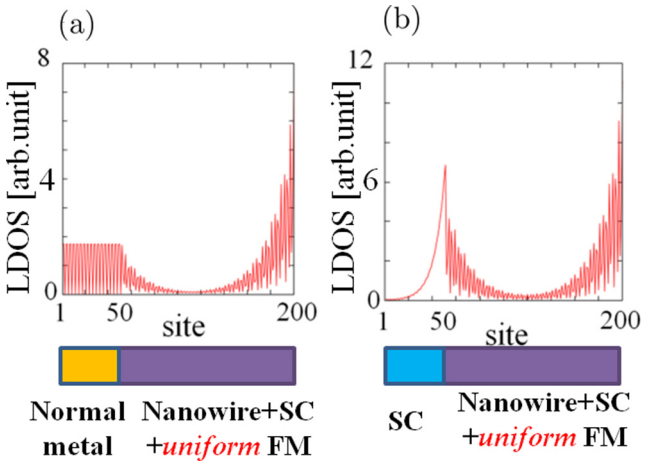

FIG. 16. (a) The spatial dependence of LDOS of the normal metal/nanowire with a pair potential and a *uniform* ferromagnetic order junction system whose length is 200 sites. The interface is positioned at 50 sites. (b) A similar plot to (a) but the normal metal is replaced by an s-wave superconductor. Schematic pictures of the junction are shown below each plot.

then finally these two zero modes hybridize [Fig. 14(c)] to split into two [Fig. 14(d)].

Below we analyze the spatial profile of LDOS of the system we consider here in more detail, especially focusing on at the zero energy. In Figs. 15(a)–15(c) we plot this spatial dependence of LDOS for several cases of decay length. For large enough ξ_L [Fig. 15(a) and 15(b)] we see the two ZEP: one is on the edge, i.e., at 200 sites, and another, which is identified as a broad peak, is left from it [for Fig. 15(a) this ZEP is located at site 140–150 and for Fig. 15(b) it is at around site 180]. We notice that the position of the left peak is shifted if the decay length is changed and accordingly the behavior of the oscillations of LDOS left from the broad peak changes. However, we also find that the oscillations between the two peaks show similar behavior. When the decay length is shorter than around $\xi_L = 20$, the two peaks hybridize and are away from the zero energy [Fig. 15(c)]. Furthermore, we also calculate the spatial dependence of LDOS of the normal metal/nanowire junction system with $\xi_L = 125$. We set the interface at the site 140. The result is shown in Fig. 15(d). The board peak which is indicated in Fig. 15(a) spreads into the normal metal.

Actually, we can regard the two ZEPs explained above as the MFs. To make this statement more convincing, we calculate the spatial profile of the LDOS of the normal metal/nanowire with a pair potential and a *uniform* ferromagnetic order junction system as well as that of an s-wave superconductor/nanowire junction system. These plots are shown in Figs. 16(a) and 16(b), respectively. The interface is located at site 50. In Fig. 15(a) the ZEP on the left, which should be expected to appear at the interface, penetrates into the normal metal segment. This is analogous to Fig. 15(d). Moreover, in Fig. 16(b) we can see the ZEP on the left (at site 50), however, as opposed to Fig. 16(a), this ZEP cannot spread into the left from the interface due to the superconducting energy gap. Therefore, ZEP cannot be stabilized and decays away from the interface. This behavior is similar to Figs. 15(a) and 15(b), however, there is one difference: in Figs. 15(a) and 15(b) due to the presence of a *nonuniform* ferromagnetic order, there is n'ot the explicit boundary which distinguishes the topologically trivial area and nontrivial one. Thus, the broad ZEP appears in Figs. 15(a) and 15(b).

The comparison between the results of Figs. 15 and 16 implies that two ZEPs appearing in a *nonuniform* case can be identified as two MFs.

[1] A. A. Golubov, M. Y. Kupriyanov, and E. Ilichev, Rev. Mod. Phys. **76**, 411 (2004).
[2] A. I. Buzdin, Rev. Mod. Phys. **77**, 935 (2005).
[3] F. S. Bergeret, A. F. Volkov, and K. B. Efetov, Rev. Mod. Phys. **77**, 1321 (2005).
[4] L. N. Bulaevskii, V. V. Kuzii, and A. A. Sobyanin, JETP Lett. **25**, 291 (1977).
[5] A. I. Buzdin, L. N. Bulaevskii, and S. V. Panyukov, JETP Lett. **35**, 178 (1982).
[6] P. Fulde and R. A. Ferrell, Phys. Rev. **135**, A550 (1964).
[7] A. I. Larkin and Yu. N. Ovchinnikov, Zh. Eksp. Teor. Fiz. **47**, 1136 (1964) [Sov. Phys. JETP **20**, 762 (1965)].
[8] V. V. Ryazanov, V. A. Oboznov, A. Y. Rusanov, A. V. Veretennikov, A. A. Golubov, and J. Aarts, Phys. Rev. Lett. **86**, 2427 (2001).
[9] T. Kontos, M. Aprili, J. Lesueur, F. Genêt, B. Stephanidis, and R. Boursier, Phys. Rev. Lett. **89**, 137007 (2002).
[10] J. W. A. Robinson, S. Piano, G. Burnell, C. Bell, and M. G. Blamire, Phys. Rev. Lett. **97**, 177003 (2006).
[11] Y. Tanaka and S. Kashiwaya, Physica C **274**, 357 (1997).
[12] H. Sellier, C. Baraduc, F. Lefloch, and R. Calemczuk, Phys. Rev. Lett. **92**, 257005 (2004).
[13] J. W. A. Robinson, S. Piano, G. Burnell, C. Bell, and M. G. Blamire, Phys. Rev. B **76**, 094522 (2007).
[14] F. S. Bergeret, A. F. Volkov, and K. B. Efetov, Phys. Rev. Lett. **86**, 4096 (2001).
[15] A. F. Volkov, F. S. Bergeret, and K. B. Efetov, Phys. Rev. Lett. **90**, 117006 (2003).
[16] M. Eschrig, Phys. Today **64**(1), 43 (2011).
[17] M. Eschrig, J. Kopu, J. C. Cuevas, and G. Schön, Phys. Rev. Lett. **90**, 137003 (2003).
[18] R. S. Keizer, S. T. B. Goennenwein, T. M. Klapwijk, G. Miao, G. Xiao, and A. Gupta, Nature (London) **439**, 825 (2006).
[19] I. Sosnin, H. Cho, V. T. Petrashov, and A. F. Volkov, Phys. Rev. Lett. **96**, 157002 (2006).
[20] T. S. Khaire, M. A. Khasawneh, W. P. Pratt, Jr., and N. O. Birge, Phys. Rev. Lett. **104**, 137002 (2010).
[21] W. A. Robinson, J. D. S. Witt, and M. G. Blamire, Science **329**, 59 (2010).
[22] D. Sprungmann, K. Westerholt, H. Zabel, M. Weides, and H. Kohlstedt, Phys. Rev. B **82**, 060505 (2010).
[23] M. S. Anwar, F. Czeschka, M. Hesselberth, M. Porcu, and J. Aarts, Phys. Rev. B **82**, 100501(R) (2010).

[24] F. S. Bergeret, A. F. Volkov, and K. B. Efetov, Phys. Rev. B **69**, 174504 (2004).
[25] F. S. Bergeret, A. Levy Yeyati, and A. Martín-Rodero, Phys. Rev. B **72**, 064524 (2005).
[26] J. Linder, T. Yokoyama, and A. Sudbø, Phys. Rev. B **79**, 054523 (2009).
[27] J. Xia, V. Shelukhin, M. Karpovski, A. Kapitulnik, and A. Palevski, Phys. Rev. Lett. **102**, 087004 (2009).
[28] R. M. Lutchyn, J. D. Sau, and S. Das Sarma, Phys. Rev. Lett. **105**, 077001 (2010).
[29] Y. Oreg, G. Refael, and F. von Oppen, Phys. Rev. Lett. **105**, 177002 (2010).
[30] M. Sato and S. Fujimoto, Phys. Rev. B **79**, 094504 (2009).
[31] A. Y. Kitaev, Usp. Fiz. Nauk (Suppl.) **171**, 131 (2001).
[32] J. Alicea, Rep. Prog. Phys. **75**, 076501 (2012).
[33] J. Alicea, Y. Oreg, G. Refael, F. von Oppen, and M. Fisher, Nat. Phys. **7**, 412 (2011).
[34] C. Nayak, S. H. Simon, A. Stern, M. Freedman, and S. Das Sarma, Rev. Mod. Phys. **80**, 1083 (2008).
[35] S. Nadj-Perge, I. K. Drozdov, B. A. Bernevig, and A. Yazdani, Phys. Rev. B **88**, 020407 (2013).
[36] S. Nadj-Perge, I. K. Drozdov, J. Li, H. Chen, S. Jeon, J. Seo, A. H. MacDonald, B. A. Bernevig, and A. Yazdani, Science **346**, 602 (2014).
[37] K. Pöyhönen, A. Westström, J. Röntynen, and T. Ojanen, Phys. Rev. B **89**, 115109 (2014).
[38] F. Pientka, L. I. Glazman, and F. von Oppen, Phys. Rev. B **89**, 180505 (2014).
[39] B. Braunecker and P. Simon, Phys. Rev. Lett. **111**, 147202 (2013).
[40] J. Klinovaja, P. Stano, A. Yazdani, and D. Loss, Phys. Rev. Lett. **111**, 186805 (2013).
[41] R. Pawlak, M. Kisiel, J. Klinovaja, T. Meier, S. Kawai, T. Glatzel, D. Loss, and E. Meyer, arXiv:1505.06078.
[42] S. Hoffman, J. Klinovaja, T. Meng, and D. Loss, Phys. Rev. B **92**, 125422 (2015).
[43] T. Meng, J. Klinovaja, S. Hoffman, P. Simon, and D. Loss, Phys. Rev. B **92**, 064503 (2015).
[44] D. Sticlet, C. Bena, and P. Simon, Phys. Rev. Lett. **108**, 096802 (2012).
[45] L. Yu, Acta Phys. Sin. **21**, 75 (1965).
[46] H. Shiba, Prog. Theor. Phys. **40**, 435 (1968).
[47] A. I. Rusinov, Zh. Eksp. Teor. Fiz. **56**, 2047 (1969) A. Rusinov, [Sov. Phys. JETP **29**, 1101 (1969)].
[48] Y. Asano and Y. Tanaka, Phys. Rev. B **87**, 104513 (2013).
[49] Y. Tanaka and S. Kashiwaya, Phys. Rev. B **56**, 892 (1997).
[50] Y. Tanaka and S. Kashiwaya, Phys. Rev. B **53**, R11957(R) (1996).
[51] S. Kashiwaya and Y. Tanaka, Rep. Prog. Phys. **63**, 1641 (2000).
[52] H. Kwon, K. Sengupta, and V. Yakovenko, Eur. Phys. J. B **37**, 349 (2004).
[53] Y. Asano, Y. Tanaka, and S. Kashiwaya, Phys. Rev. Lett. **96**, 097007 (2006).
[54] K. T. Law and P. A. Lee, Phys. Rev. B **84**, 081304 (2011).
[55] L. J. Buchholtz and G. Zwicknagl, Phys. Rev. B **23**, 5788 (1981).
[56] J. Hara and K. Nagai, Prog. Theor. Phys. **76**, 1237 (1986).
[57] C. R. Hu, Phys. Rev. Lett. **72**, 1526 (1994).
[58] Y. Tanaka and S. Kashiwaya, Phys. Rev. Lett. **74**, 3451 (1995).
[59] Y. Tanaka and S. Kashiwaya, Phys. Rev. B **53**, 9371 (1996).
[60] C. W. J. Beenakker, Annu. Rev. Condens. Matter Phys. **4**, 113 (2013).
[61] S. Yip, J. Low Temp. Phys. **91**, 203 (1993).
[62] Y. S. Barash, H. Burkhardt, and D. Rainer, Phys. Rev. Lett. **77**, 4070 (1996).
[63] V. L. Berezinskii, JETP Lett. **20**, 287 (1974).
[64] A. M. Black-Schaffer and A. V. Balatsky, Phys. Rev. B **87**, 220506 (2013).
[65] Y. Tanaka, A. A. Golubov, S. Kashiwaya, and M. Ueda, Phys. Rev. Lett. **99**, 037005 (2007).
[66] Y. Tanaka, M. Sato, and N. Nagaosa, J. Phys. Soc. Jpn. **81**, 011013 (2012).
[67] M. Eschrig, T. Löfwander, T. Champel, J. Cuevas, and G. Schön, J. Low Temp. Phys. **147**, 457 (2007).
[68] Y. Asano, Y. Tanaka, and A. A. Golubov, Phys. Rev. Lett. **98**, 107002 (2007).
[69] V. Braude and Y. V. Nazarov, Phys. Rev. Lett. **98**, 077003 (2007).
[70] Y. Asano, Y. Sawa, Y. Tanaka, and A. A. Golubov, Phys. Rev. B **76**, 224525 (2007).
[71] M. Eschrig and T. Löfwander, Nat. Phys. **4**, 138 (2008).
[72] Y. Tanaka, Y. Tanuma, and A. A. Golubov, Phys. Rev. B **76**, 054522 (2007).
[73] S. V. Bakurskiy, A. A. Golubov, M. Y. Kupriyanov, K. Yada, and Y. Tanaka, Phys. Rev. B **90**, 064513 (2014).
[74] R. Wakatsuki, M. Ezawa, Y. Tanaka, and N. Nagaosa, Phys. Rev. B **90**, 014505 (2014).
[75] H. Ebisu, K. Yada, H. Kasai, and Y. Tanaka, Phys. Rev. B **91**, 054518 (2015).
[76] X. Liu, J. D. Sau, and S. Das Sarma, Phys. Rev. B **92**, 014513 (2015).
[77] Y. Tanaka and A. A. Golubov, Phys. Rev. Lett. **98**, 037003 (2007).
[78] A. Pal, Z. H. Barber, J. W. A. Robinson, and M. G. Blamire, Nat. Commun. **5**, 3340 (2014).
[79] Y. Tanaka and S. Kashiwaya, Phys. Rev. B **70**, 012507 (2004).
[80] Y. Tanaka, S. Kashiwaya, and T. Yokoyama, Phys. Rev. B **71**, 094513 (2005).
[81] Y. Tanaka, Y. Asano, A. A. Golubov, and S. Kashiwaya, Phys. Rev. B **72**, 140503(R) (2005).
[82] T. Yokoyama, Y. Tanaka, and A. A. Golubov, Phys. Rev. B **75**, 134510 (2007).
[83] T. Yokoyama, Y. Tanaka, and N. Nagaosa, Phys. Rev. Lett. **106**, 246601 (2011).